Available online at www.sciencedirect.com

ScienceDirect

Geochimica et Cosmochimica Acta 124 (2014) 309–327

Geochimica et Cosmochimica Acta

www.elsevier.com/locate/gca

Morphology and crystal structures of solar and presolar Al_2O_3 in unequilibrated ordinary chondrites

Aki Takigawa [a,*,1], Shogo Tachibana [a,2], Gary R. Huss [b], Kazuhide Nagashima [b], Kentaro Makide [b,3], Alexander N. Krot [b], Hiroko Nagahara [a]

[a] Department of Earth and Planetary Science, The University of Tokyo, 7-3-1 Hongo, Tokyo 113-0033, Japan
[b] Hawai'i Institute of Geophysics and Planetology, School of Ocean, Earth Science and Technology, Honolulu, HI 96822, USA

Received 18 May 2013; accepted in revised form 11 September 2013; available online 23 September 2013

Abstract

Corundum, the thermodynamically stable phase of alumina (Al_2O_3), is one of the most refractory dust species to condense around evolved stars. Presolar alumina in primitive chondrites has survived various kinds of processing in circumstellar environments, the interstellar medium (ISM), the Sun's parent molecular cloud, and the protosolar disk. The morphology and crystal structure of presolar alumina grains may reflect their formation and evolution processes, but the relative importance of these two types of processes is poorly understood. In this study, we performed detailed morphological observations of 185 alumina grains extracted from unequilibrated ordinary chondrites (Semarkona, Bishunpur, and RC075). We also performed electron back-scattered diffraction analyses of 122 grains and oxygen isotopic analyses of 107 grains. Dissolution experiments on corundum and transition alumina phases were carried out to examine the possibility of the alteration of surface structures of alumina grains by the chemical separation procedures of chondrites.

The average size of the alumina grains was 1 μm, and neither whiskers nor extremely flat grains were observed. About one-third of the grains had smooth surfaces, while ~60% of the grains had rough surfaces with 10–100 nm-sized fine structures. The rough-surface grains have varieties of morphology and crystallinity, suggesting that the rough surface structures are secondary in origin. Electron back-scattered diffraction patterns from 95% of alumina grains matched with α-Al_2O_3 (corundum), and more than 75% of the alumina grains are single crystals of corundum. Nine presolar alumina grains with anomalous oxygen isotopic compositions were found among 107 alumina grains, and most of them were characterized by rough surface structures. While most of the presolar alumina grains were corundum, the relative abundance of amorphous or low-crystallinity grains is higher in presolar alumina grains than in solar alumina grains. The dissolution experiments showed that all phases except for corundum dissolved during the acid treatments of chondrites. This suggests that smooth surface structures of corundum grains were originally formed in space, and that original surfaces of alumina that had been damaged by energetic particle irradiation in the ISM or the protosolar disk were lost during chemical separations to form the rough surface structures, and that amorphous or low-crystallinity alumina grains in chondrites have acid-resistant structures different from sol–gel-synthesized amorphous alumina. The present results also imply the possible presence of acid-soluble alumina phases, undiscovered by chemical separations, in chondrites.

* Corresponding author. Present address: Carnegie Institution of Washington, Department of Terrestrial Magnetism, 5241 Broad Branch Road NW, Washington, DC 20015, USA. Tel.: +1 202 478 8463.

E-mail addresses: takigawa@kueps.kyoto-u.ac.jp, atkigawa@ciw.edu (A. Takigawa), tachi@ep.sci.hokudai.ac.jp (S. Tachibana), ghuss@higp.hawaii.edu (G.R. Huss), kazu@higp.hawaii.edu (K. Nagashima), makide.kentaro@musashi.ed.jp (K. Makide), sasha@higp.hawaii.edu (A.N. Krot), hiroko@eps.s.u-tokyo.ac.jp (H. Nagahara).

[1] Present address: Department of Geology and Mineralogy, Kyoto University, Kitashirakawa Oiwake-cho, Kyoto 606-8502, Japan.
[2] Present address: Department of Natural History Sciences, Hokkaido University, N10 W8, Sapporo 060-0810, Japan.
[3] Present address: Musashi Senior and Junior High School, 1-26-1 Toyotamakami, Nerima, Tokyo 176-8535, Japan.

0016-7037/$ - see front matter © 2013 Elsevier Ltd. All rights reserved.
http://dx.doi.org/10.1016/j.gca.2013.09.013

1. INTRODUCTION

Primitive chondrites include small quantities of presolar grains that show highly unusual isotopic compositions compared to solar-system materials (e.g., Zinner, 2007 and references therein). More than 250 Al_2O_3 (alumina) grains of presolar origin have been reported previously (Hutcheon et al., 1994; Huss et al., 1994; Nittler et al., 1994, 1997, 2008; Choi et al., 1998, 1999; Nguyen et al., 2003, 2007; Zinner et al., 2003, 2005; Mostefaoui and Hoppe, 2004; Nagashima et al., 2004; Floss and Stadermann, 2009; Makide et al., 2009; Bose et al., 2010; Gyngard et al., 2010; Leitner et al., 2012). Their oxygen isotopic compositions indicate that most of them came from oxygen-rich red giants or AGB (asymptotic giant branch) stars. Infrared spectroscopic observations of oxygen-rich AGB stars show broad features with a peak at ~11–12 μm, which are explained by the presence of amorphous or γ-alumina around these stars (e.g., Onaka et al., 1989; Speck et al., 2000). Each of these spectra often accompanies a single narrow peak at 13 μm, which is not explained by crystalline silicates and may be emitted by crystalline oxides. The specific origin of the 13 μm peak has not yet been determined, but corundum and spinel are proposed to be the most plausible candidates by the works on laboratory-measured or calculated spectra of dust analogues (Posch et al., 1999; Fabian et al., 2001; Takigawa et al., 2012).

Corundum, which is the only thermodynamically stable phase of alumina (Al_2O_3), is one of the first condensates from a gas of solar composition based on equilibrium condensation calculations (e.g., Grossman, 1972; Davis and Richter, 2003). Alumina is the dominant component among highly refractory minerals predicted to form in the system of solar composition (cf., the solar elemental ratio of Al/Si = 0.08), and could thus play an important role as seed nuclei for formation of less refractory minerals such as silicates and iron metal at lower temperatures.

Thermodynamic equilibrium calculations predict that alumina is replaced by other phases at lower temperature, but the presence of presolar alumina grains and the possible presence of alumina dust in circumstellar outflows from evolved stars suggest that alumina grains survived processes in circumstellar dust-forming environments, the interstellar medium (ISM), and the protosolar disk.

The physical and chemical conditions of mineral formation and alteration are likely to be preserved in chemistry, crystal structure and morphology of minerals. Due to their retention of large isotopic anomalies, presolar alumina grains are expected to record the conditions of dust formation in circumstellar outflows and of alteration due to energetic particle irradiation in the ISM (and possibly in the early solar system). The isotopic compositions of presolar alumina grains have been used to constrain their stellar sources. Presolar alumina grains are often referred to as "presolar corundum (α-Al_2O_3)", but Stroud et al. (2004, 2007) reported that three presolar alumina grains had structures of corundum, amorphous alumina, and an unidentified phase of Al_2O_3. The discovery of presolar non-corundum alumina is consistent with the infrared observation of a broad feature at ~11–12 μm for oxygen-rich AGB stars, and also implies the formation of alumina dust under non-equilibrium conditions and/or alteration of crystal structures by ion irradiation.

Just as euhedral presolar grains such as a platy hibonite in Semarkona (LL3.0) ordinary chondrite (Choi et al., 1999) and SiC grains in Murchison (CM2) carbonaceous chondrite (Amari et al., 1994; Bernatowicz et al., 2003) may reflect their formation processes, alumina grains could also retain the morphology formed during condensation in circumstellar environments. Moreover, grain morphology has a significant influence on the infrared absorption/emission spectrum of circumstellar dust grains (Takigawa et al., 2012; Takigawa and Tachibana, 2012). Choi et al. (1998) observed alumina grains from the acid residues of chondrites prior to isotopic measurements by ion microprobe and pointed out that presolar alumina grains in unequilibrated ordinary chondrites (UOCs) have distinctive irregular surfaces and often appear to be aggregates of smaller grains. They also showed that most of the alumina grains with the solar system O-isotopic compositions have smooth surfaces and a few have crystal faces, while some grains have irregular surface structures. Such irregular surface structures appeared to be <100 nm in size. Makide et al. (2009) investigated O-isotopic compositions of relatively large alumina grains (>5 μm) from UOCs and found one presolar alumina grain with an irregular surface structure.

These studies suggest that there seems to be variations in crystal structure and morphology of both solar and presolar alumina grains, but they have not been systematically studied because the abundance of presolar alumina in chondrites is low (0.2–30 ppm, Nguyen et al., 2007) and because most of the presolar alumina grains have been found by destructive isotope mapping of the residues of chemical treatments of chondrites (e.g., Nittler et al., 1997).

Another potential problem in investigation of crystal structure and morphology of alumina grains in chondrites is that chemical treatments of chondrites to extract the grains may affect the grain properties in the acid residues. For instance, Bernatowicz et al. (2003) showed that 60% of presolar SiC grains isolated by physical disaggregation without any chemical treatments from Murchison (CM2) carbonaceous chondrite appear to be coated with a thin (<100 nm) layer of an apparently very fine-grained or an amorphous material. These layers were not observed for the SiC grains isolated by the chemical treatments (Amari et al., 1994) and may have been removed by the treatments. The coatings may have originated through oxidation of the surfaces of SiC grains to silica under the oxidizing condition in the protosolar disk (Mendybaev et al., 2002). Alumina grains may also suffer from modification of morphology and surface structures and selective dissolution of less resistant material during the acid treatments.

In this study, in order to systematically investigate morphology and crystal structures of both presolar and solar alumina grains and to clarify the characteristics of presolar alumina, we made detailed observations of shapes, surface structures, and crystallinity of alumina grains from acid residues of unequilibrated ordinary chondrites prior to destructive ion-probe measurements of their oxygen isotopic compositions. We also performed dissolution experiments on synthetic alumina polymorphs to evaluate

the effect of the chemical treatments on the morphological and crystallographic properties of alumina grains in the meteorite acid residues.

2. SAMPLES AND EXPERIMENTAL METHODS

2.1. Morphological, crystallographic, and isotopic analyses of alumina grains from UOCs

Acid-residues of UOCs, Semarkona (LL3.0), Bishunpur (LL3.1), and Roosevelt County (RC) 075 (H3.2), prepared by Huss and Lewis (1995) and Huss et al. (1998), were used for this study. The residues, consisting mostly of acid-resistant grains such as corundum, spinel, hibonite, and SiC, were suspended in a mixture of 90% isopropanol and 10% water and dispersed onto gold substrates cleaned by ion milling. Four gold substrates were prepared in this study (1 for Semarkona, 1 for Bishunpur, and 2 for RC075). Alumina candidate grains were found by cathodoluminescence mapping using a JEOL JXA-8500F field-emission electron microprobe equipped with a Gatan MiniCL detector at University of Hawai'i at Manoa, and 198 alumina grains were identified by energy dispersive spectroscopy (EDS) using a JEOL JSM-7000F field-emission scanning microscope (FE-SEM) at University of Tokyo.

Grains found to have agglomerated with spinel, SiC grains, or other Al_2O_3 grains during the dispersion process were eliminated from further analyses. We also eliminated those with nearby grains within a 30 μm area because a primary ion beam defocused to ~30 μm was used for ion-microprobe oxygen-isotope analyses. Overall, 185 alumina grains were selected for this study, among which 25, 73, and 87 grains were from Semarkona, Bishunpur, and RC 075, respectively (Table 1).

In order to study the morphology of each grain, secondary electron images were taken from four different directions by tilting and rotating the sample stage of the FE-SEM; the stage tilt angle and the anticlockwise rotation angle of (0°, 0°) [*top*], (70°, 0°) [*front*], (70°, 90°) [*left*], and (70°, 270°) [*right*] (Fig. 1). Because the ~1-μm-sized grains were dispersed on the gold substrate, no conductive coating was required for the SEM observation.

The electron back-scattered diffraction (EBSD) pattern of each grain was obtained with an HKL EBSD system mounted on the FE-SEM. Measurements were made with the stage tilt angle and the rotation angle of (70°, 0°). The working distance was 15 mm, the acceleration voltage was 15 kV, and the beam current was 5–13 nA. The configuration of the SEM sample stage and the EBSD detector for EBSD analyses is schematically shown in Fig. 2. The regions surrounded by the solid curves in Fig. 2 are illuminated by the electron beam, and those surrounded by the dashed curves are visible to the EBSD detector and the nominal position for EBSD analysis (rotation = 0°, tilt = 70°). The region within both the dashed and solid curves is thus the region where back-scattered electrons can be detected by the EBSD detector. The fraction of the grain accessible to EBSD measurements to the whole grain surface depends on grain morphology. Roundish and/or thorny grains (e.g., RC075 59-07) tend to have larger shaded regions than flatter grains (e.g., Bishunpur 60-02). Note also that grains even with similar shapes and/or surface morphologies may have different fractions of accessible regions depending on the positional relation to the incident electron beam and the detector.

The EBSD patterns of the polycrystalline gold substrate nearby each individual grain were also measured because an EBSD pattern coming from the gold substrate beneath the grain often overlapped with the EBSD pattern of the target grain due to its small size and roundish shape. Kikuchi bands of a target grain were determined manually by comparing the EBSD patterns of the grain and of the surrounding gold substrate, and the crystal orientation was indexed by comparing the determined Kikuchi bands with simulated EBSD patterns of corundum. The averaged angular misfit (Mean Angular Deviation: MAD) between the determined and simulated Kikuchi bands of <1.0° was used as the criteria for successful indexing. EBSD analyses were performed for more than three locations on an individual grain for 122 grains and for a single location for each of the other 53 grains (Table 1).

Oxygen isotopic compositions of 107 grains (Table 1) were measured with the Cameca ims-1280 ion-microprobe at University of Hawai'i following the analytical procedure of Makide et al. (2009). A 0.5–2.5 nA Cs^+ primary ion beam was defocused to ~30 μm in diameter for uniform sputtering of an individual grain irrespective of its morphology and size (0.6–3 μm). A field aperture of

Table 1
Number of alumina grains studied for morphology, crystallography, and oxygen isotopes.

Meteorite	FE-SEM	EBSD						SIMS
		Multiple locations					Single location	
		Single crystal α-Al_2O_3[a]	Polycrystalline α-Al_2O_3[b]	Single EBSP of α-Al_2O_3[c]	Low-crytsallinity[d]	Amorphous[e]	α-Al_2O_3	
Bishunpur	73	55	7	1	1	0	2	49
RC075	87	37	3	10	7	1	29	50
Semarkona	25	0	0	0	0	0	18	8
Total	185	92	10	11	8	1	50	107

[a] Identical EBSD patterns of α-Al_2O_3 from all measured locations.
[b] More than one EBSD patterns of α-Al_2O_3.
[c] An EBSD pattern of α-Al_2O_3 from one location and no clear EBSD patterns from other locations.
[d] Only EBSD patterns with MAD > 1.
[e] No EBSD patterns.

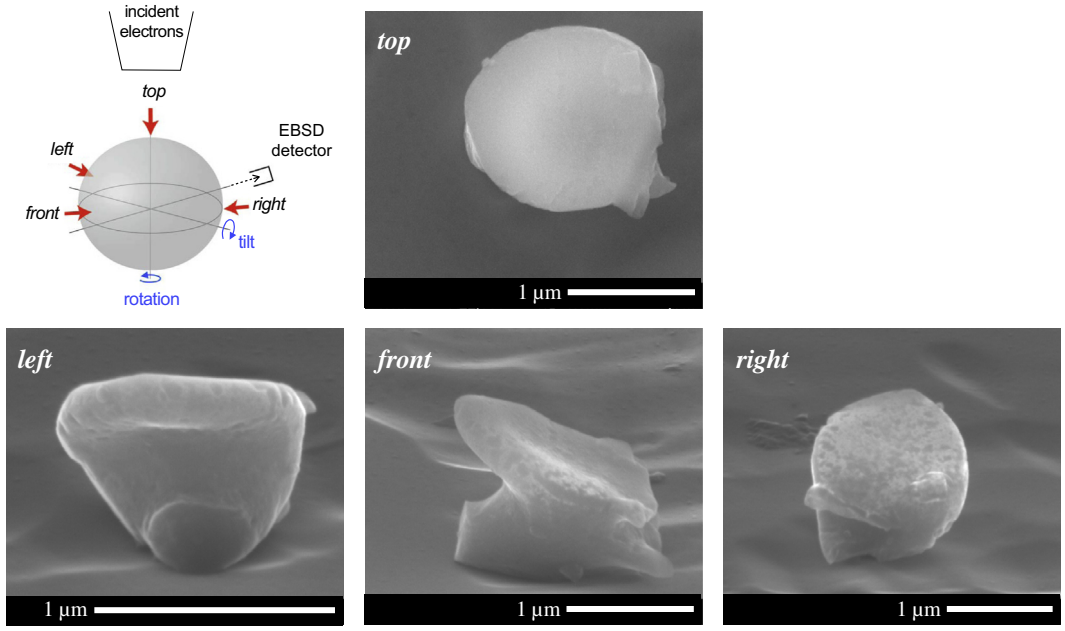

Fig. 1. The positional relation of the incident electrons, tilting and rotation axes of the SEM stage, and EBSD detector and an example of secondary electron images of an alumina grain (Bishunpur 60-34) taken from four directions. Secondary electron images from *top*, *front*, *right*, and *left* directions were taken by rotating and tilting the SEM stage. The stage tilt angles and the anticlockwise rotation angles of *top*, *front*, *right*, and *left* directions are (0°, 0°), (70°, 0°), (70°, 90°) and (70°, 270°), respectively.

$1500 \times 1500\ \mu m^2$, corresponding to $\sim 10 \times 10\ \mu m^2$ on the sample, was used to minimize contribution of oxygen signals from the gold substrate and other grains located close to the grain of interest. Secondary $^{16}O^-$, $^{17}O^-$, and $^{18}O^-$ ions were measured in multicollection mode with the magnetic field controlled by a nuclear magnetic resonance probe. $^{16}O^-$ and $^{18}O^-$ were measured with a multicollector Faraday cup and Electron Multiplier (EM), respectively, with mass resolving power (MRP) of ~2000, and $^{17}O^-$ was measured using the axial monocollector EM with MRP of ~5600 to separate the interfering $^{16}OH^-$ signal. The primary beam current was adjusted to obtain $^{16}O^-$ signal of $>\sim 10^6$ cps. One to ten micron-sized Burma spinel grains dispersed on a gold substrate were used as the standard. Acquisition time was typically 200 s (10 s × 20 cycles), but it was reduced to 50–130 s (10 s × 5–13 cycles) during analyses for grains showing presolar oxygen isotopic signatures to keep grains from being completely sputtered. The count rates of oxygen isotopes tend to monotonically decrease during analyses due to consumption of grains, and in the data reduction process, cycles with the $^{17}O^-$ count rate of <100 cps were not used because they have large statistical uncertainties for $\Delta^{17}O$ ($= \delta^{17}O - 0.52 \times \delta^{18}O$). Note that this threshold ($^{17}O^-$ of <100 cps) was arbitrary but the threshold value does not affect the identification of presolar alumina grains.

2.2. Dissolution experiments of alumina polymorphs

2.2.1. Sample preparation

Alpha-alumina (corundum) is the only stable phase of aluminum oxide, and there are several polymorphs known as transition alumina. Alpha-alumina and transition alumina are divided into two groups based on the packing of oxygen in their crystal structures; γ (cubic), η (cubic), θ (monoclinic), and δ (tetragonal or orthorhombic) alumina have face-centered cubic (fcc) unit cells, and α (trigonal), κ (orthorhombic), χ (hexagonal) alumina have hexagonal close-packed (hcp) unit cells (Levin and Brandon, 1998). All the transition alumina phases can be present at room temperature, but irreversible phase transitions occur with increasing temperature. They are transformed to α-alumina by heating at 1100 °C for a few hours.

For dissolution experiments, we used α-alumina, prepared by grinding a single crystal of corundum synthesized by the Kyropoulos method (Dalian Keri Opt. Tech.), and a commercial reagent of α-alumina formed by dehydration of aluminum hydroxide (Taimei Chemicals). Transition alumina powders were synthesized by dehydration of aluminum hydroxide (gibbsite ($Al(OH)_3$)) and aluminum oxide hydroxide (böhmite (AlOOH)) following the procedures of Day and Hill (1953), Wefers and Misra (1987), and Fukuyama et al. (2009). Kappa- and χ-alumina were obtained by dehydration of gibbsite (Wako Chemicals) at 600 and 900 °C in a muffle furnace in the air for 24 h. Böhmite was synthesized by hydrothermal treatment of gibbsite at 200 °C and 2 MPa for 24 h in a hydrothermal Teflon vessel. Gamma-, δ-, and θ-alumina were obtained by dehydration of the synthesized böhmite at 600, 900, and 1000 °C in a muffle furnace in the air for 24 h. A commercial reagent of γ-alumina (Wako Chemicals) was also used in the experiments.

Amorphous alumina grains were obtained by a sol–gel method using aluminum alkoxide as a starting material (Ono and Matsuno 2004). Aluminum tri-sec-butoxide ($Al(C_4H_9O)_3$) was dissolved into ethyl acetate ($CH_3COOCH_2CH_3$) to be 0.4 mol/l. Two moles of acetic acid per mole of aluminum tri-sec-butoxide and 2 cm^3 of ethanol

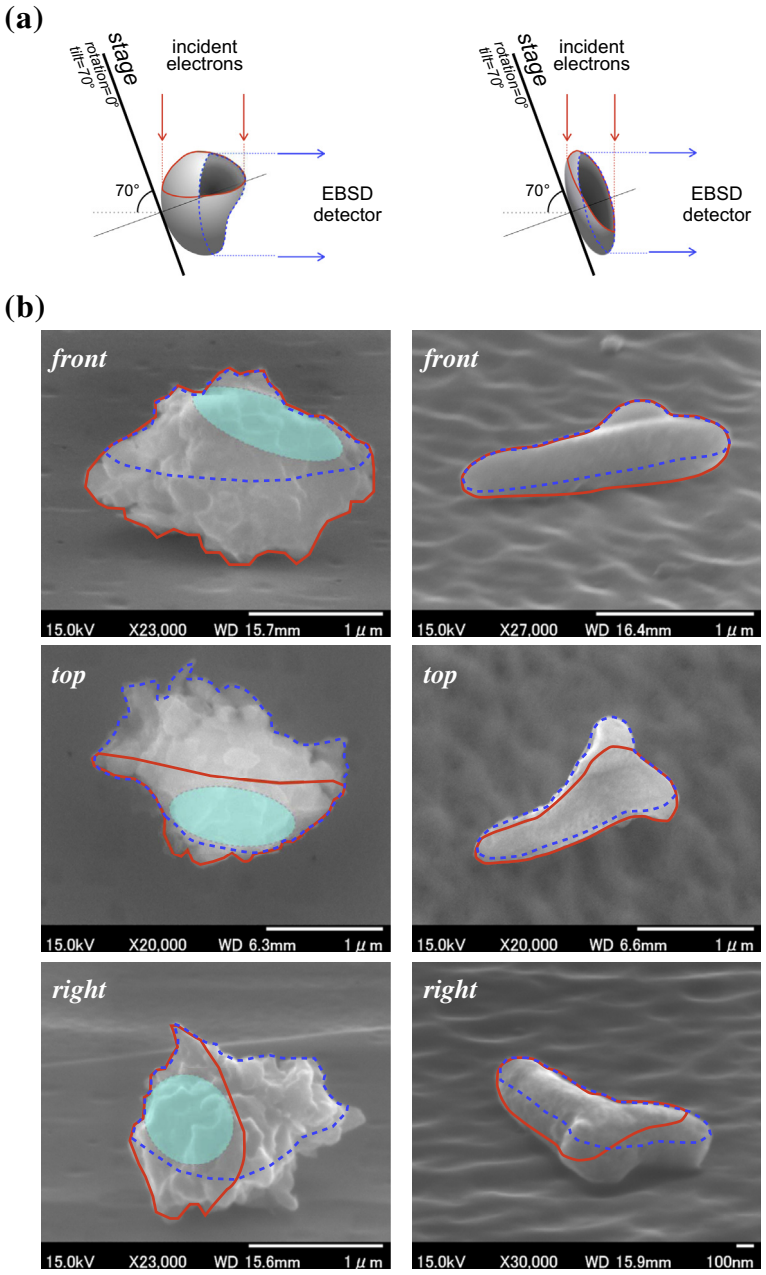

Fig. 2. The positional relation of alumina grains relative to incident electrons and the EBSD detector during EBSD measurements. The stage position is the same as the *front* direction for morphological observation (Fig. 1). The detector is behind the sample, and the stage is tilted so that the sample faces toward the detector. (a) Schematic illustrations of roundish and flat grains with regions illuminated by incident electrons (surrounded by solid curves) and visible to the EBSD detector (surrounded by dashed curves). EBSD patterns can be obtained only from the region within both curves. Flat grains tend to have a larger accessible region than roundish and/or thorny grains. (b) Examples of regions illuminated by incident electrons and visible the EBSD detector for roundish (RC075 59-07) and flat (Bishunpur 60-02) grains for EBSD analyses at the *front* stage positions. The same regions are also shown in secondary electron images taken from the *top* and *right* directions. The EBSD pattern of RC075 59-07 shown in Fig. 8 was obtained from the area indicated by the light blue. (For interpretation of the references to colour in this figure legend, the reader is referred to the web version of this article.)

for every cm^3 of ethyl acetate were added to the solution. The solution was then mixed at ~80 °C to obtain a homogeneous precursor solution. Homogeneous gel powder was then obtained by evaporating the solvent of ethyl acetate and ethanol at ~80 °C. The net reaction of the sol–gel method is

$$2Al(OBu)_3 + 3H_2O \rightarrow Al_2O_3 + 6BuOH \ , (CH_3COOH + CH_3CH_2OH = CH_3COOC_2H_5 + H_2O),$$

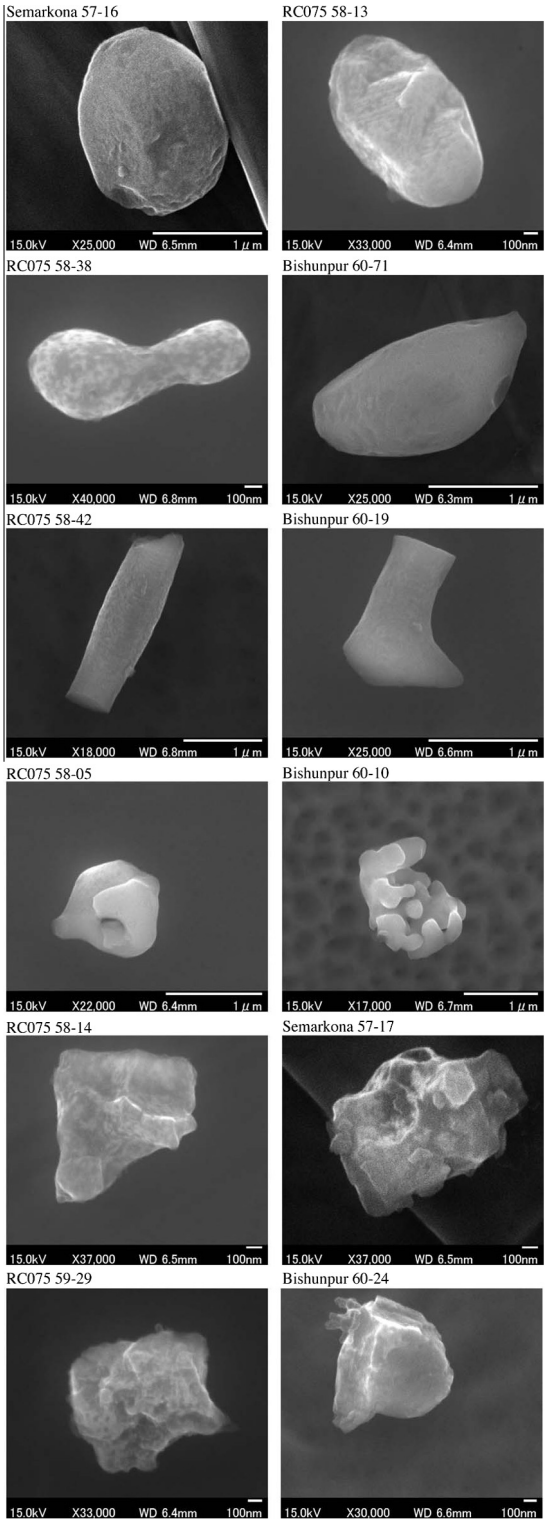

Fig. 3. Secondary electron images of alumina grains with different morphologies; Equant shape (Semarkona 57-16 and RC075 58-13), droplet-like shape (RC075 58-38 and Bishunpur 60-71), broken-droplet like shape (RC075 58-42 and Bishunpur 60-19), botryoidal shape (RC075 58-05 and Bishunpur 60-10), and irregular shapes (RC075 58-14, Semarkona 57-17, RC075 59-29, and Bishunpur 60-24). All the images were taken from the *top* direction.

where $Al(OBu)_3$ is aluminum tri-sec-butoxide and BuOH is butanol. The synthesized gel powders were heated at 500 °C in the air for 2 h to obtain amorphous alumina powders. All the products were analyzed by X-ray powder diffraction (XRD; PANalytical X'Pert Pro MPD) and Fourier Transform Infrared Spectroscopy (FT-IR; JASCO FT/IR-4200).

2.2.2. Dissolution experiments

The dissolution experiments on the alumina particles were conducted following the treatment procedure of Huss and Lewis (1995), the procedure by which the acid residues of UOCs used in this study were prepared. In this study, three acid treatments were performed for α- and commercial γ-alumina; (1) 12 M HF – 6 M HCl at room temperature for 10 days, (2) 2 M H_2SO_4 + 0.5 N $K_2Cr_7O_4$ at 75 °C for 12 h, and (3) $HClO_4$ at 190–200 °C for 2 h. In the HF/HCl treatment by Huss and Lewis (1995), the acid was changed every 24 h to provide enough capacity to dissolve the entire sample while minimizing the total fluid volume. These acid-cycle steps were simplified in this study because only alumina powders were processed with a much higher acid/sample ratio than Huss and Lewis (1995). The commercial γ-alumina was also treated in 12 M HF – 6 M HCl for 15 h, in 12 M HF for 24 h, and in 6 M HCl for 24 h, respectively, at room temperature.

All the acid treatments were performed in Teflon microtubes (1.5 ml). About 1 mg of alumina powder was put in the microtube with the acid (or acid mixture) of ~1 ml. The alumina and the acid were well mixed by ultrasonification before each acid treatment step. After each treatment, the microtube was centrifuged to separate solid components from the acid and the acid was pipetted out. The residual solid material was rinsed twice by adding purified water into the microtube and by ultrasonification prior to the next acid treatment. The microtubes were placed in an incubator during the acid treatments (2) and (3) to keep the temperatures constant. The synthesized transition alumina (χ, δ, γ, κ, and θ alumina) and amorphous alumina grains disappeared in 12 M HF – 6 M HCl at room temperature in 24 h, which was ten times shorter than the actual duration for the acid treatments of chondrites.

After the acid treatment, a fraction of the residual solid was well mixed with ethanol by ultrasonification, and the mixture was dispersed onto aluminum foil for observation with the FE-SEM.

3. RESULTS

3.1. Morphology, crystal structures and oxygen isotopes of alumina grains in UOCs

3.1.1. Shape, size, and surface structures

Secondary electron images of 185 alumina grains from Semarkona, Bishunpur, and RC 075 were taken from the *top*, *front*, *left*, and *right* directions (Fig. 1), and images of several grains are shown in Fig. 3 (the images of all grains are in Fig. S1 (Supplementary material)). The longest and shortest dimensions of each of these grains, which were measured through the apparent center of mass of the grain

in four SE images, are shown in Fig. 4. The ratios of the shortest to the longest dimension of most grains range from 0.25 to 0.75, and neither whiskers nor extremely flat grains are present. The frequency distribution of grain size (Fig. 5), which is denoted by the average of the longest and shortest dimensions, shows that there is no grain larger than 3.0 μm in size and gives the mode of 1.0 μm and the mean size of 1.2 μm. However, it should be noted that alumina grains smaller than 0.6 μm were also present on the mounts but were excluded from this study and that the mode and mean size reported here are the upper limits. We also note that the ratio of the shortest to the longest dimensions and the size distribution of alumina in the three chondrites do not differ from one another. The size information for individual grains is summarized in Table S1.

The grains show a variety of shapes (Figs. 3 and S1). Fig. 3 shows characteristic shapes of the grains; equant, typically with crystal faces (e.g., Semarkona 57-16 and RC075 58-13), droplet-like shapes (e.g., RC075 58-38 and Bishunpur 60-71), broken-droplet like shapes, which might be fragments of larger grains (e.g., RC075 58-42 and Bishunpur 60-19), botryoidal shapes (e.g., Bishunpur 60-10 and RC075 58-05), and irregular shapes (e.g., RC075 58-14, Semarkona 57-17, RC075 59-29, Bishunpur 60-24).

The grains also show a variety of surface structures (Fig. 6). About one-third of the grains have smooth surfaces, while the remaining two-third of the grains have rough surfaces with 10–100 nm-sized fine structures that look similar to the grains reported by Choi et al. (1998) and Makide et al. (2009). The surface roughness seems to be unrelated to the shape. For instance, both RC075 59-22 (Fig. 6d) and Semarkona 57-26 (Fig. 6h) show similar highly rough surfaces, but they have different outer shapes (equant and broken-droplet). There are also some grains with similar outer shapes, but showing different degrees of surface roughness from smooth to highly rough (Fig. 7). Moreover, the 10–100 nm-sized surface features show structural variety; some rough grains have fluffy and edgy fine surface structures (Fig. 7a), while some have blunt and roundish fine structures (Fig. 7b).

3.1.2. Crystal structures

We measured EBSD patterns of 172 grains from at least one position on each grain. The results of EBSD analyses for individual grains are summarized in Tables 1 and S1. An example of EBSD pattern of an alumina grain (RC075 59-07) is shown in Fig. 8 with that of the surrounding Au substrate. The EBSD pattern obtained from RC075 59-07 differs clearly from that of the Au substrate, and matches with α-Al_2O_3.

As described in the Section 2.1, EBSD patterns of the grains were obtained only from the region that is simultaneously illuminated by the incident electron beam and visible to the EBSD detector (Fig. 2a and b). Identical EBSD patterns of α-Al_2O_3 (Fig. 8a) were obtained from the area indicated by light blue on RC075 59-07 (Fig. 2b). However, only the EBSD pattern of the Au substrate (Fig. 8b) was observed from the left side of the light blue region possibly due to a thin edge of the grain. It was often difficult to obtain EBSD patterns near edges of the grains because EBSD patterns from the surrounding Au substrate overwhelmed those from the grains.

For the 122 grains from Bishunpur and RC075, EBSD patterns were measured at multiple locations of the grain surface. Identical EBSD patterns of α-Al_2O_3 were obtained from multiple surface locations for 92 grains (SC(M), Table S1), suggesting that at least 75% of the alumina

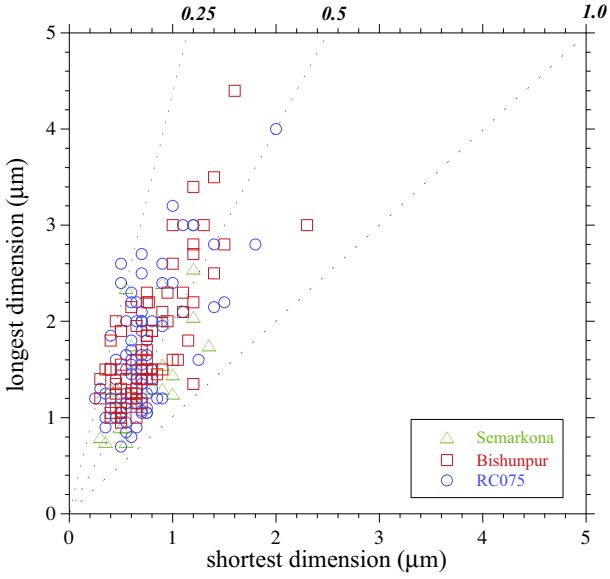

Fig. 4. The longest and shortest dimensions of 185 alumina grains in Semarkona, RC075, and Bishunpur. Dotted lines show the ratios of the shortest to longest dimensions of 0.25, 0.5, and 1.

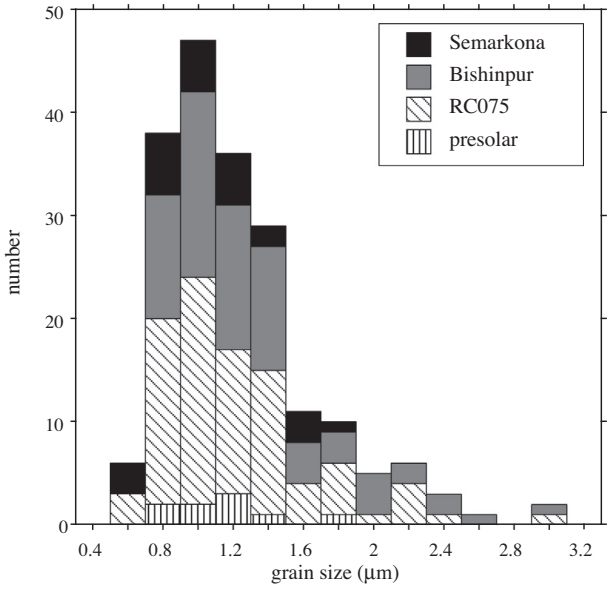

Fig. 5. Frequency distribution of the average size (the mean of the longest and shortest dimensions) of 185 alumina grains in Semarkona, RC075, and Bishunpur. Data for presolar alumina grains found in this study are shown separately.

grains were single crystals of corundum. We should note that we cannot fully exclude that some of the grains are polycrystalline because the EBSD patterns were not obtained from the entire surfaces of the grains. More than one crystal patterns were observed from 10 grains (PC(M), Table S1). This implies that they were polycrystalline α-Al_2O_3.

For 11 grains among those for which EBSD patterns were measured at multiple locations, an EBSD pattern of α-Al_2O_3 was obtained only from one location, but no clear EBSD pattern was observed from other locations (SE(M), Table S1). For five of these grains (RC075 58-04, 59-02, 59-06, and 59-15, and Bishunpur 60-63), the areas from which we could expect to get EBSD patterns are small due to their thin, sharp or tapered edges (Fig. S1). The other grains (RC075 58-17, 58-29, 58-49, 59-03, 59-29, and Bishunpur 60-68) have large regions that should give EBSD patterns if they were crystalline, but did not display clear EBSD patterns within the regions except for single locations. These observations indicate that crystallinity of the regions where no clear EBSD patterns were observed is actually low and that the crystallinity may not be uniform within these six grains. Only relatively weak EBSD patterns with MAD > 1 were obtained for 8 grains (LC(M), Table S1; RC075 58-02, RC075 58-09, RC075 58-22, RC075 58-46, RC075 58-52, RC075 59-01, RC075 59-08, and Bishunpur 60-23). This could be due to grain morphology for four grains (RC075 58-22, 58-26, and 59-01, and Bishunpur 60-23) (Fig. S1), but the other four grains (RC075 58-02, 58-09, 58-52, and 59-08) do not have any geometrical features responsible for the weak Kikuchi bands. Since clear EBSD patterns were obtained from other grains with similar morphology, the latter four grains could be low-crystallinity corundum or transition alumina phases with low crystallinity. No Kikuchi band was obtained for one grain (AM(M), Table S1; RC075 58-48). This cannot be attributed to the grain morphology, and the grain could thus be amorphous alumina.

For each of 50 grains, an EBSD pattern was measured at a single location and all the patterns matched those of α-

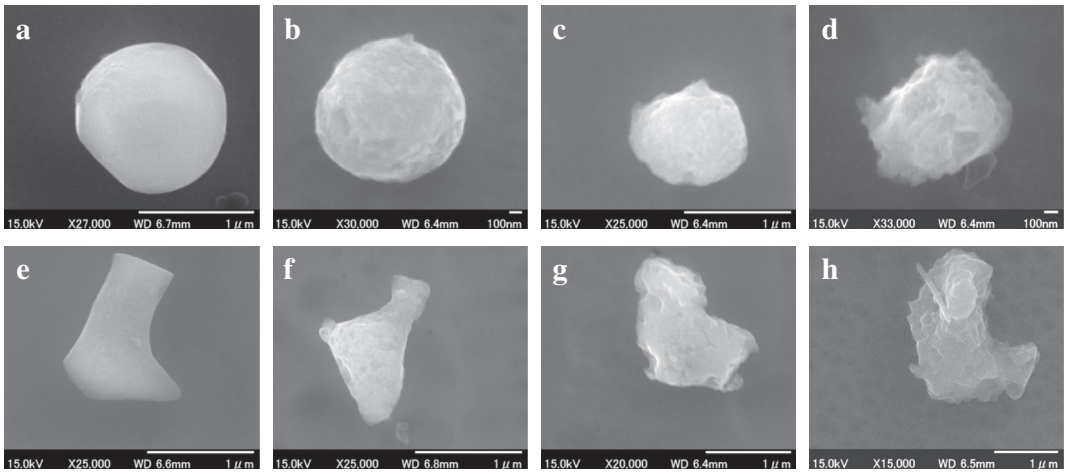

Fig. 6. Comparison of surface structures of equant shaped grains ((a)–(d)) and broken-droplet shaped grains ((e)–(h)). Grains with similar outer shapes show different degrees of surface roughness from smooth to highly rough. (a) Bishunpur 60-64, (b) RC075 59-17. (c) RC075 59-04. (d) RC075 59-22. (e) Bishunpur 60-19. (f) RC075 58-36. (g) RC075 58-12. (h) Semarkona 57-19.

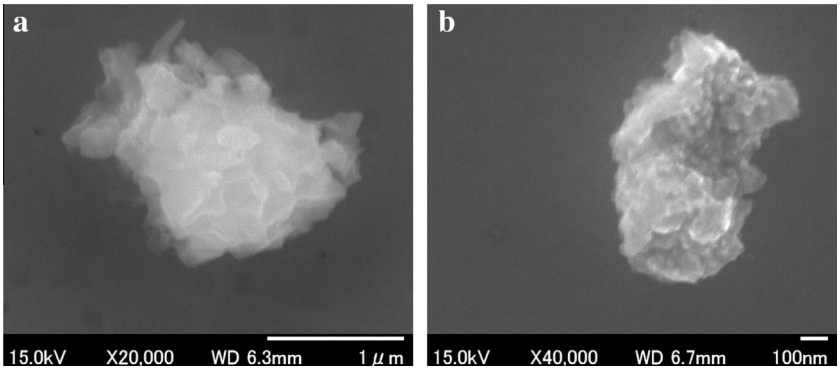

Fig. 7. Structural variety of 10–100 nm-sized surface rough features. Some grains have fluffy and edgy fine surface structures as (a) RC075 59-07 and some have blunt and roundish fine structures as (b) Semarkona 57-26.

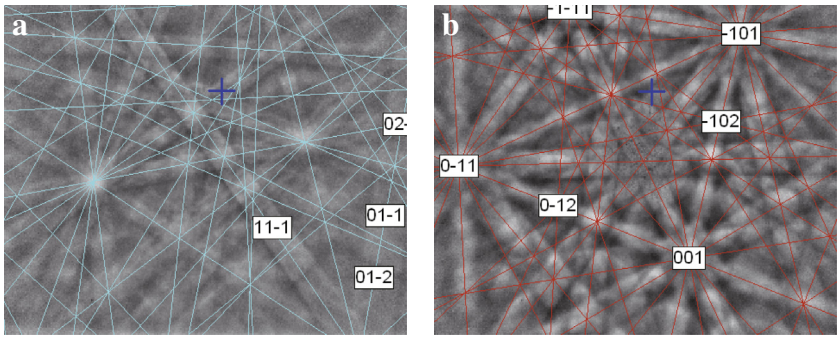

Fig. 8. An example of EBSD patterns from an alumina grain (RC075 59-07, Fig. 2) (a) and from a surrounding Au substrate (b). The EBSD pattern of the grain is matched with α-Al_2O_3.

Al_2O_3 (C(S), Table S1). Because only one pattern was measured for those grains, it is not clear whether they are single crystals, or polycrystalline.

In summary, the EBSD patterns from 95% of the grains (163 grains) matched those of α-Al_2O_3, and thus most of the alumina grains found from UOCs in this study are at least partly corundum.

3.1.3. Oxygen isotopic compositions

The oxygen isotopic compositions of 107 alumina grains (8, 43, and 47 grains from Semarkona, Bishunpur, and RC075, respectively) are shown as deviations from SMOW (Standard Mean Ocean Water), $\delta^{17}O$ *vs.* $\delta^{18}O$, in Fig. 9. The oxygen isotopic compositions of individual grains are given in Table S1. Most of the grains have oxygen isotopic compositions that plot near the Carbonaceous Chondrite Anhydrous Mineral (CCAM) line, indicating that they originated in the solar system. Some data plotted along the terrestrial fractionation (TF) line. For these grains, the oxygen compositions could be indigenous, but may possibly be analytical artifacts (e.g., geometric effects of grain-surface roughness or adsorbed terrestrial water on the gold substrate). If such ^{18}O-rich materials were present during analyses, some data plotted near the CCAM line but slightly at the ^{18}O-rich side might also be explained by mixing with them. Further experiments are needed to confirm the presence of such contaminants or geometrical effects on instrumental mass fractionation, but we should note that such effects do not affect the identification of anomalous oxygen isotopic signatures of presolar alumina grains. Among 107 grains we measured, nine presolar alumina grains having oxygen isotopic anomalies were found (~8% of measured grains; Fig. 9; Table 2); seven are from RC075 (RC075 58-09, RC075 58-33, RC075 58-49, RC075 59-07, RC075 59-08, RC075 59-09, and RC075 59-22) and two are from Bishunpur (Bishunpur 60-35 and Bishunpur 60-44). RC075 58-33 showed the clear presolar signature for the first six cycles (Table 2), but the anomalous signal disappeared during the analysis and the grain had been completely sputtered after the measurements. The $^{17}O^-$ signal dropped below 100 cps at the tenth cycle due to its small grain size. The data reduction was made for the first nine cycles, and the data for RC075 58-33 shown in Fig. 9 and Table 2 has relatively larger uncertainties because it includes both presolar and solar isotopic signatures.

Seven presolar grains (RC075 58-33, RC075 59-07, RC075 59-08, RC075 59-09, RC075 59-22, Bishunpur 60-35, and Bishunpur 60-44) show positive ^{17}O excesses and small ^{18}O depletions (Fig. 8), and these oxygen isotopic signatures are explained by the first dredge-up in red giants (Nittler et al., 1997). They are classified into Group I based on the classification scheme of Zinner (2005), while according to Nittler et al. (1997), RC075 59-09 with the smallest ^{17}O excess is classified as Group III (grains originated from low-mass and low-metallicity red giants) and RC075 58-33 with the second smallest ^{17}O excess is in between Group I and III in terms of ^{17}O excess. Two grains (RC075 58-09 and RC075 58-49) show ^{17}O depletions, which are classified as Group III grains (Nittler et al., 1997, Zinner, 2005).

3.2. Dissolution properties of alumina polymorphs

The phases of synthesized alumina powders were confirmed by XRD and FT-IR (Figs. 10 and 11) compared with the data reported by Zhou and Synder (1991), Begemann et al. (1997), Santos et al. (2000), Webster et al. (2005), Boumaza et al. (2009), and Favaro et al. (2010).

Secondary electron images of the starting α-alumina grains and those after the dissolution treatment through (1) to (3) (Fig. 12) showed that no significant change occurred for the surface structures of α-alumina grains.

Commercial γ-alumina particles were, on the other hand, completely dissolved after the first step of acid procedures (12 M HF – 6 M HCl at room temperature for 10 days). The same acid treatment for 15 h, which was one sixteenth of the duration of the treatment (1), was done for commercial γ-alumina, where the number of particles significantly decreased, the average size of the remaining particles became smaller than that of the starting powders, and their morphology were turned into roundish (Fig. 12). These lines of evidence suggest rapid dissolution of γ-alumina into the acid. Additional dissolution experiments of commercial γ-alumina in 12 M HF and in 6 M HCl for 24 h showed that γ-alumina dissolves especially into HF. We also found that γ-alumina dissolves in some degree dur-

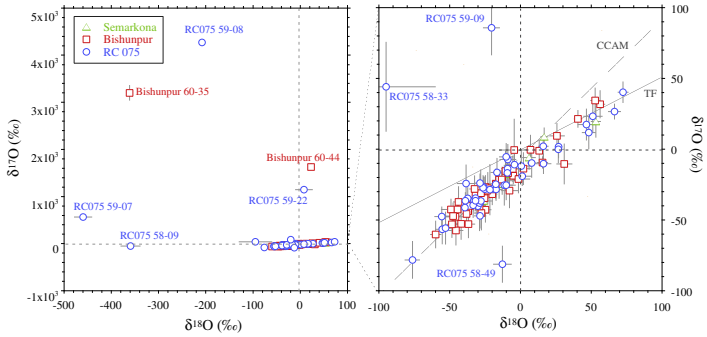

Fig. 9. Oxygen isotopic compositions of 109 alumina grains from UOCs (pink: Bishunpur; light blue: RC075; light green: Semarkona). The isotopic compositions are expressed as differences from that of SMOW (standard mean ocean water); $\delta^{i}O$ (‰) = $(({}^{i}O/{}^{16}O)_{sample}/({}^{i}O/{}^{16}O)_{SMOW}\text{-}1) \times 1000$ ($i = 17$ or 18). The terrestrial mass fractionation (TF) line and the carbonaceous chondrite anhydrous mineral (CCAM) line are also shown. Error bars are 2-sigma.

ing the treatment (2) (2 M H_2SO_4 + 0.5 N $K_2Cr_7O_4$ at 75 °C for 12 h) and dissolves effectively during the treatment (3) ($HClO_4$ at 190–200 °C for 2 h).

Secondary electron images of synthesized transition alumina particles (χ, δ, γ, κ, and θ alumina) are shown in Fig. 13 with those of gibbsite and böhmite, from which transition alumina phases were synthesized. Gibbsite particles are equant, while böhmite particles have platy rhombic shapes. The transition alumina phases produced by dehydration of gibbsite and böhmite seem to take over the morphologies of their precursor phases, respectively. The amorphous alumina grains synthesized by the sol–gel method were very fine (<100 nm in size) and agglomerated (Fig. 13).

The acid treatment of the synthetic transition alumina and amorphous alumina in 12 M HF – 6 M HCl at room temperature for 24 h showed that κ- and amorphous alumina grains were completely dissolved into the acid. The other synthetic phases (χ-, γ-, δ-, and θ-alumina) were mostly dissolved into the acid; the remaining particles of χ-, γ-, δ-, and θ-alumina were much less and much smaller than the starting particles and their edges were highly rounded (Fig. 14). This result indicates that these alumina phases would be almost completely dissolved during the actual acid treatments done for meteorites.

The dissolution rates of minerals change with the abundances of defects and kinks, where the bonds are energetically easily broken (e.g., Carroll-Webb and Walther, 1988). The fact that all of the synthesized transition alumina showed broader and weaker XRD and FT-IR peaks than those of corundum (Figs. 10 and 11) indicates that the sizes of crystallites are smaller for transition alumina and the length and/or vibration frequency of the Al–O bond have a variety in some degree. There are thus a number of weak Al–O bonds in the structures of transition alumina, which is likely to lead to the enhanced dissolution rates of transition alumina into the acid.

4. DISCUSSION

4.1. Morphology, crystal structures, and relative abundance of presolar alumina grains

We first discuss morphological and crystallographic features of nine presolar alumina grains and their relationship (Fig. 15 and Table 2).

Table 2
Oxygen isotopic compositions of presolar alumina grains.[a]

Meteorite	Grain No.	$\delta^{17}O$ (‰)	$\delta^{18}O$ (‰)	$^{17}O/^{16}O$	$^{18}O/^{16}O$	EBSD[b]
Bishunpur	60-35	3204.4 ± 31.7	−361.6 ± 3.3	$1.61(\pm0.01) \times 10^{-3}$	$1.28(\pm0.01) \times 10^{-3}$	Single EBSD pattern of α-Al_2O_3
Bishunpur	60-44	1629.8 ± 47.9	22.9 ± 6.1	$1.01(\pm0.02) \times 10^{-3}$	$2.05(\pm0.01) \times 10^{-3}$	Polycrystalline α-Al_2O_3
RC075	58-09	−44.7 ± 17.9	−381.5 ± 7.7	$3.63(\pm0.04) \times 10^{-4}$	$1.28(\pm0.04) \times 10^{-3}$	Low crystallinity
RC075	58-33[c]	44.1 ± 31.8	−95.0 ± 35.0	$4.00(\pm0.12) \times 10^{-4}$	$1.81(\pm0.01) \times 10^{-3}$	Single crystal α-Al_2O_3 w/subgrain
RC075	58-49	−81.2 ± 12.9	−12.8 ± 6.5	$3.52(\pm0.05) \times 10^{-4}$	$1.98(\pm0.01) \times 10^{-3}$	Single EBSD pattern of α-Al_2O_3
RC075	59-07	567.9 ± 17.3	−459.9 ± 18.8	$6.00(\pm0.07) \times 10^{-4}$	$1.08(\pm0.04) \times 10^{-3}$	Single crystal α-Al_2O_3
RC075	59-08	4275.2 ± 51.3	−208.2 ± 4.8	$2.02(\pm0.02) \times 10^{-3}$	$1.59(\pm0.01) \times 10^{-3}$	Low crystallinity
RC075	59-09	85.8 ± 19.4	−20.5 ± 6.0	$4.16(\pm0.07) \times 10^{-4}$	$1.96(\pm0.01) \times 10^{-3}$	Single crystal α-Al_2O_3 w/subgrain
RC075	59-22	1147.8 ± 54.2	7.6 ± 18.6	$8.22(\pm0.21) \times 10^{-4}$	$2.02(\pm0.04) \times 10^{-3}$	Single crystal α-Al_2O_3

[a] All errors are 2σ.
[b] See details in Table 1.
[c] Isotopic compositions for the first 6 cycles are ($\delta^{17}O$, $\delta^{18}O$) = (70.5 ± 26.7‰, −124.8 ± 26.2‰), corresponding to ($^{17}O/^{18}O$, $^{18}O/^{18}O$) = ($4.10(\pm0.10) \times 10^{-4}$, $1.75(\pm0.05) \times 10^{-3}$).

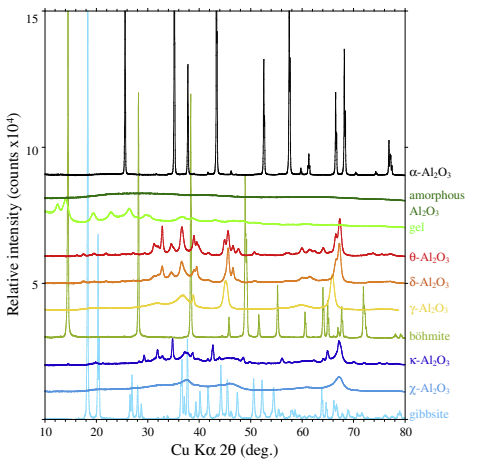

Fig. 10. XRD spectra of gibbsite ($Al(OH)_3$), χ-alumina, κ-alumina, böhmite (AlO(OH)), γ-alumina, δ-alumina, θ-alumina, alumina gel, amorphous alumina, and α-alumina (corundum). Alpha-alumina and γ-alumina are commercial reagents from Taimei Chemicals and Wako Chemicals. Each spectrum is shifted by a fixed offset of 50,000 counts.

RC075 59-08 (Fig. 15a), RC075 59-07 (Fig. 15b), and Bishunpur 60-35 (Fig. 15c) had very irregular outer shapes with fine surface features. Bishunpur 60-35 showed a weak EBSD pattern matching α-Al_2O_3 from a single location of the grain before the SIMS analysis, and the same EBSD patterns were obtained from multiple locations after the measurement, which suggests that the grain is a single crystal of corundum. RC59-07 and RC59-08 had similar rough surface structures, but their crystallinities were different. RC59-07 is a single crystal of corundum showing identical EBSD patterns of α-Al_2O_3 from multiple points before and after the isotopic analysis. This grain did not show any indications of crystal faces, and the outer shape did not show any relation with the crystallographic orientation (Fig. 15b). On the other hand, only a single very weak pattern was obtained from RC075 59-08 before the SIMS measurement; the pattern was not observed after the measurement. This indicates that crystallinity of the grain is low. The fact that outer shapes of presolar grains do not correlate with their crystallinity implies that different processes are responsible for these two features.

RC075 59-22 (Fig. 15d) and RC075 58-09 (Fig. 15e) are subhedral grains and have rough surface structures. RC075 58-09 showed no Kikuchi band in the EBSD analysis at all before SIMS analysis, but a single very faint Kikuchi band was observed after the SIMS analysis. RC075 58-09 is thus likely to be mostly amorphous with a small region of a defect-rich and low-crystallinity structure inside. RC075 59-22 showed an identical crystalline EBSD pattern of α-Al_2O_3 from multiple surface locations prior to the SIMS measurement (i.e., a single crystal of corundum). The arrow in Fig. 15d shows the orientation of the c-axis and the relatively smooth surface perpendicular to the c-axis observed from the *right* direction corresponds to a crystal face of {0001}. The same EBSD pattern was obtained after the isotopic analysis as well, but the contrast of Kikuchi bands was much weaker, probably due to the damage of the surface crystal structure by ion irradiation during the SIMS analysis. These two grains with similar subhedral morphology but different crystallographic structures imply that they formed as a single crystal but later experienced different alteration histories.

Bishunpur 60-44 (Fig. 15f) and RC075 58-49 (Fig. 15g) are flattened grains and have similar (footprint-like) outer shapes. However, the surface of Bishunpur 60-44 is rougher than that of RC075 58-49. RC075 58-49 showed faint Kiku-

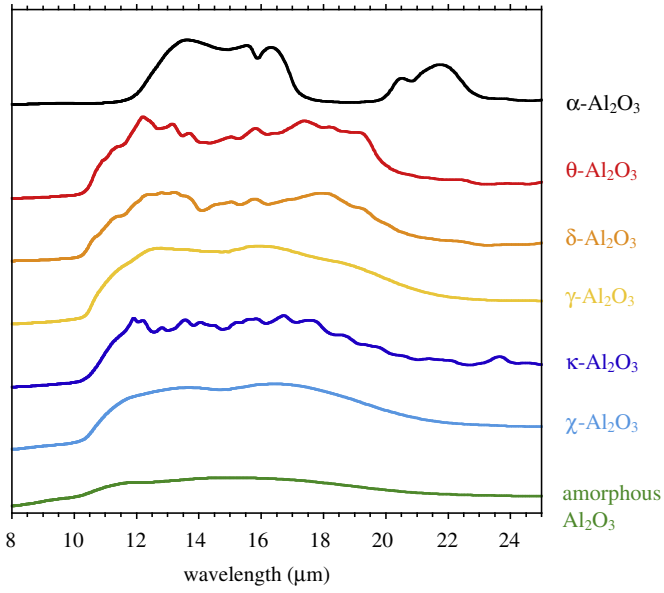

Fig. 11. Infrared absorption spectra of alumina polymorphs and amorphous alumina embedded in KBr. The unit of the vertical axis is arbitrary.

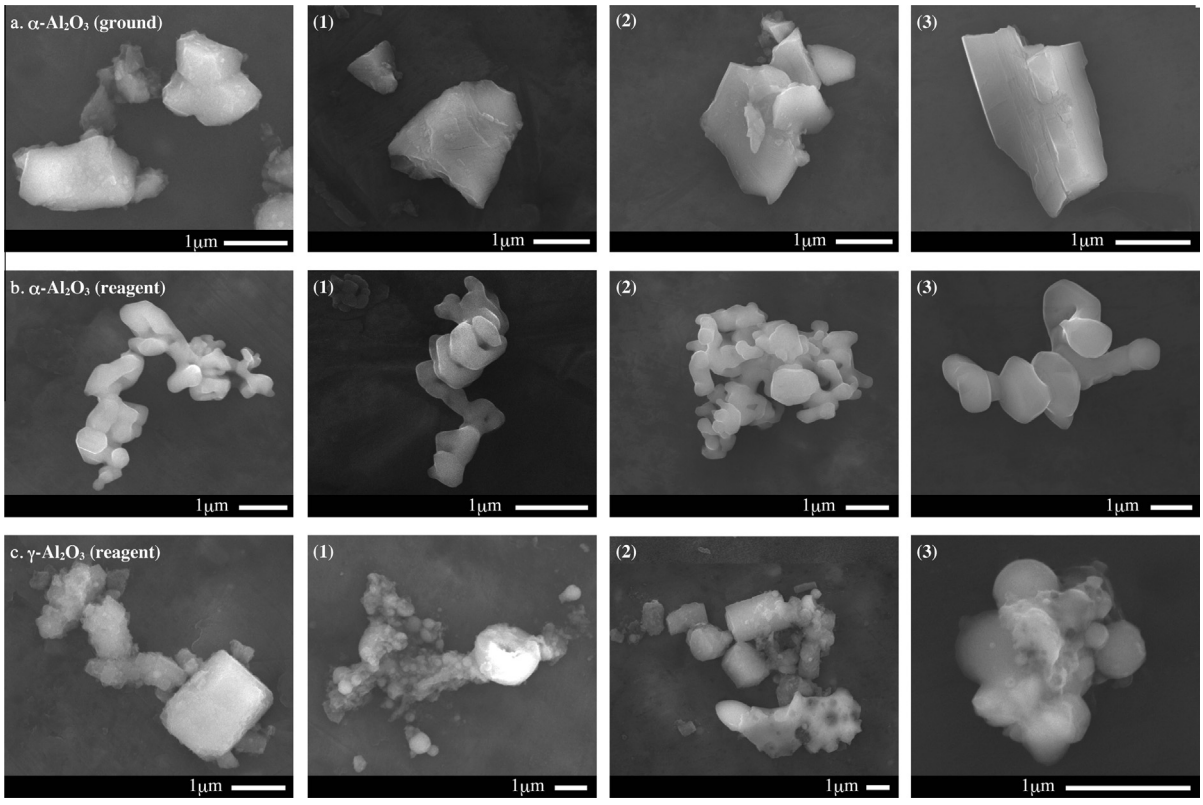

Fig. 12. Morphological changes of α-Al_2O_3 and γ-Al_2O_3 after dissolution experiments. (a) Secondary electron images of starting α-Al_2O_3 particles prepared by grinding a single crystal of synthetic corundum and those after the successive treatments of (1) 12 M HF – 6 M HCl at 25 °C for 10 days, (2) 2 M H_2SO_4 + 0.5 N $K_2Cr_7O_4$ at 75 °C for 12 h, and (3) $HClO_4$ at 190–200 °C for 2 h. (b) Secondary electron images of commercial α-Al_2O_3 particles formed by dehydration of aluminum hydroxide and those after the same successive acid treatments as in (a). No significant morphological changes were seen for α-Al_2O_3 samples irrespective of synthesis methods. (c) Secondary electron images of commercial reagent of γ-Al_2O_3 particles and those after each acid treatment of (1) 12 M HF – 6 M HCl at 25 °C for 15 h, (2) 2 M H_2SO_4 + 0.5 N $K_2Cr_7O_4$ at 75 °C for 12 h, and (3) $HClO_4$ at 190–200 °C for 2 h. Significant morphological changes were observed for γ-Al_2O_3.

chi bands, corresponding to the EBSD pattern of α-Al_2O_3 from only one location on the grain surface both before and after the SIMS measurement. Bishunpur 60-44 showed two distinct EBSD patterns of α-Al_2O_3 from different surface locations, indicating that the grain is polycrystalline. There are several possible formation mechanisms of a polycrystalline presolar Al_2O_3 grain; (1) Coagulation of individually-condensed corundum grains in a circumstellar envelope prior to condensation of other dust species such as silicates. (2) Heterogeneous nucleation and growth of Al_2O_3 on an early condensate of alumina grain in a circumstellar envelope. (3) Crystallization of amorphous Al_2O_3 grain in polycrystalline form due to thermal annealing either in a circumstellar envelope or in the protosolar disk. Although further study including dust formation kinetics in an expanding stellar envelope is required, the polycrystalline nature of Bishunpur 60-44 may put some constraints on nucleation and growth of highly refractory dust particles in outflows of red giants.

Both RC075 58-33 (Fig. 15h) and RC075 59-09 (Fig. 15i) consist of main-grains with smooth surfaces and accompanied by smaller sub-grains. The other 7 presolar grains have neither apparently accompanying grains nor smooth surfaces. The larger main grain of RC075 58-33 is found to be a single crystal of corundum by EBSD analyses. The sub-grain of RC075 58-33 is 200 nm in size and seems to have rough surface structures. The presolar oxygen isotopic anomaly from RC075 58-33 disappeared during the measurement, and the solar oxygen isotopic composition was obtained in the latter part of the analysis, which implies that either a main or a sub-grain had a presolar isotopic signature and the other does not. Although both of main- and sub-grains were completely sputtered away during the isotopic analysis, it seems likely that the smaller sub-grain with rough surface structures had a presolar origin.

RC075 59-09 is composed of a main grain of single crystal of corundum and several <100-nm-sized sub-grains. Both the main- and sub-grains survived sputtering during the isotopic measurement (Fig. 16). The sub-grain indicated by arrows in Fig. 16 showed weak Kikuchi bands different from those of the main corundum grain and the surrounding Au although the phase of the sub-grain could not be determined. By analogy with RC075 58-33, either the main or the sub-grain(s) may be presolar in origin. However, it is difficult to determine which grain (or both) has a presolar

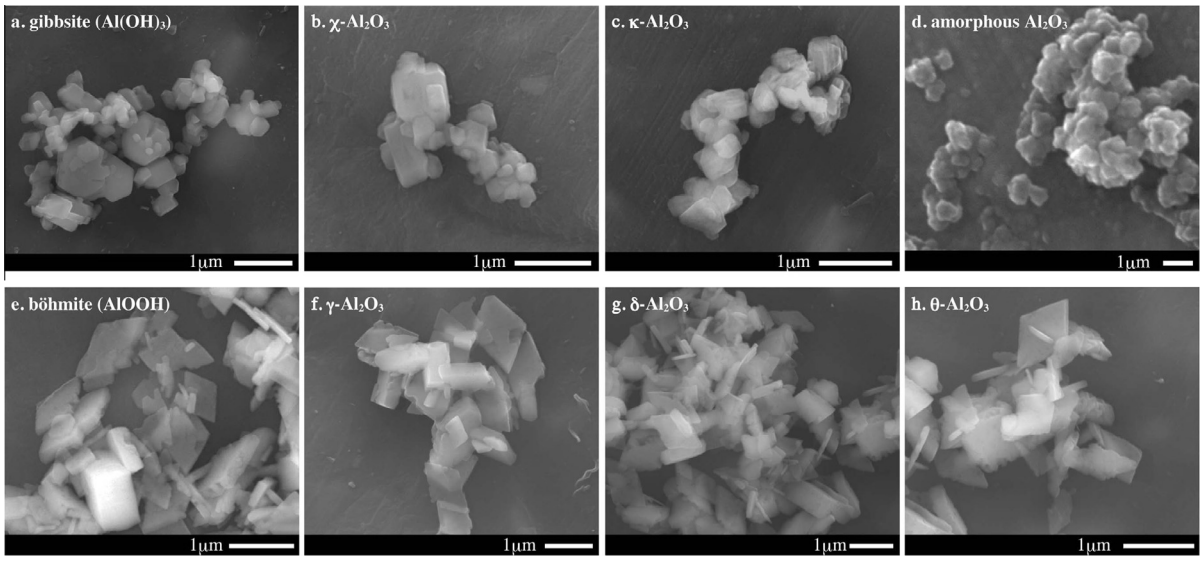

Fig. 13. Secondary electron images of alumina polymorphs synthesized from gibbsite and böhmite and sol–gel-formed amorphous alumina. (a) gibbsite. (b) χ-Al_2O_3. (c) κ-Al_2O_3. Chi (χ)-Al_2O_3 and κ-Al_2O_3 were synthesized from gibbsite. (d) amorphous alumina. (e) böhmite. (f) γ-Al_2O_3. (g) δ-Al_2O_3. (h) θ-Al_2O_3. Gamma (γ)-Al_2O_3, δ-Al_2O_3, and θ-Al_2O_3 were synthesized from böhmite.

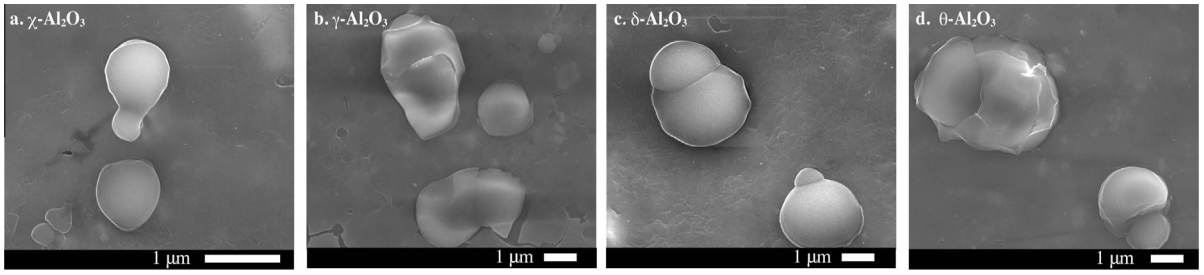

Fig. 14. Morphological changes of transition alumina powders after the acid treatment in 12 M HF – 6 M HCl at 25 °C for 24 h. (a) χ-Al_2O_3. (b) γ-Al_2O_3. (c) δ-Al_2O_3. (d) θ-Al_2O_3. κ-Al_2O_3 and amorphous alumina were completely dissolved into the acid.

origin at present, and a future isotopic measurement with higher spatial resolution is required.

Except for the grains with sub-grains (RC075 58-33 and RC075 59-09), other seven presolar grains have rough surface structures, which is consistent with the observation by Choi et al. (1998). We also note that approximately 60% of solar alumina grains have rough surface structures similar to the presolar grains. This similarity would be explained if the same process worked to form the rough surface structures of solar and presolar grains. We also found that rough-surface presolar alumina grains showed varieties of morphology from subhedral to irregular and of crystallinity from monocrystalline corundum to amorphous. The independent relationship of surface roughness to morphology and crystallinity suggests that the formation process of surface rough structures is not the same as the processes responsible for the grain morphology and crystallinity and could be secondary.

Among presolar alumina grains, the fraction of low-crystallinity or amorphous alumina grains (2 out of 7 grains) is higher than that for solar alumina grains, where 6% of the grains with EBSD measurements on multiple locations showed either low-crystallinity or amorphous features (7 out of 115 grains). The presence of low-crystallinity and amorphous presolar alumina grains is consistent with the finding of amorphous presolar alumina by Stroud et al. (2004, 2007). The difference in the corundum fraction between solar and presolar alumina grains implies either that the formation of low-crystallinity or amorphous alumina is more favorable in outflows from low mass stars than in the early solar system, or that the destruction of crystalline structures of alumina grains occurred in the ISM as occurred for ISM silicates.

The typical size of grains measured in the present study and in Choi et al. (1998) was about 1 μm (Fig. 3), while Makide et al. (2009), who measured only larger grains (1–5 μm), found only 1 probable presolar grain among 103 grains. Most of presolar alumina grains in Tieschitz (H3.6) are reported to be <1.5 μm (Nittler et al., 1997), consistent with the present result (Fig. 3).

Eight percent of the alumina grains (9 out of 107 grains) were found to be presolar in this study. This relative abun-

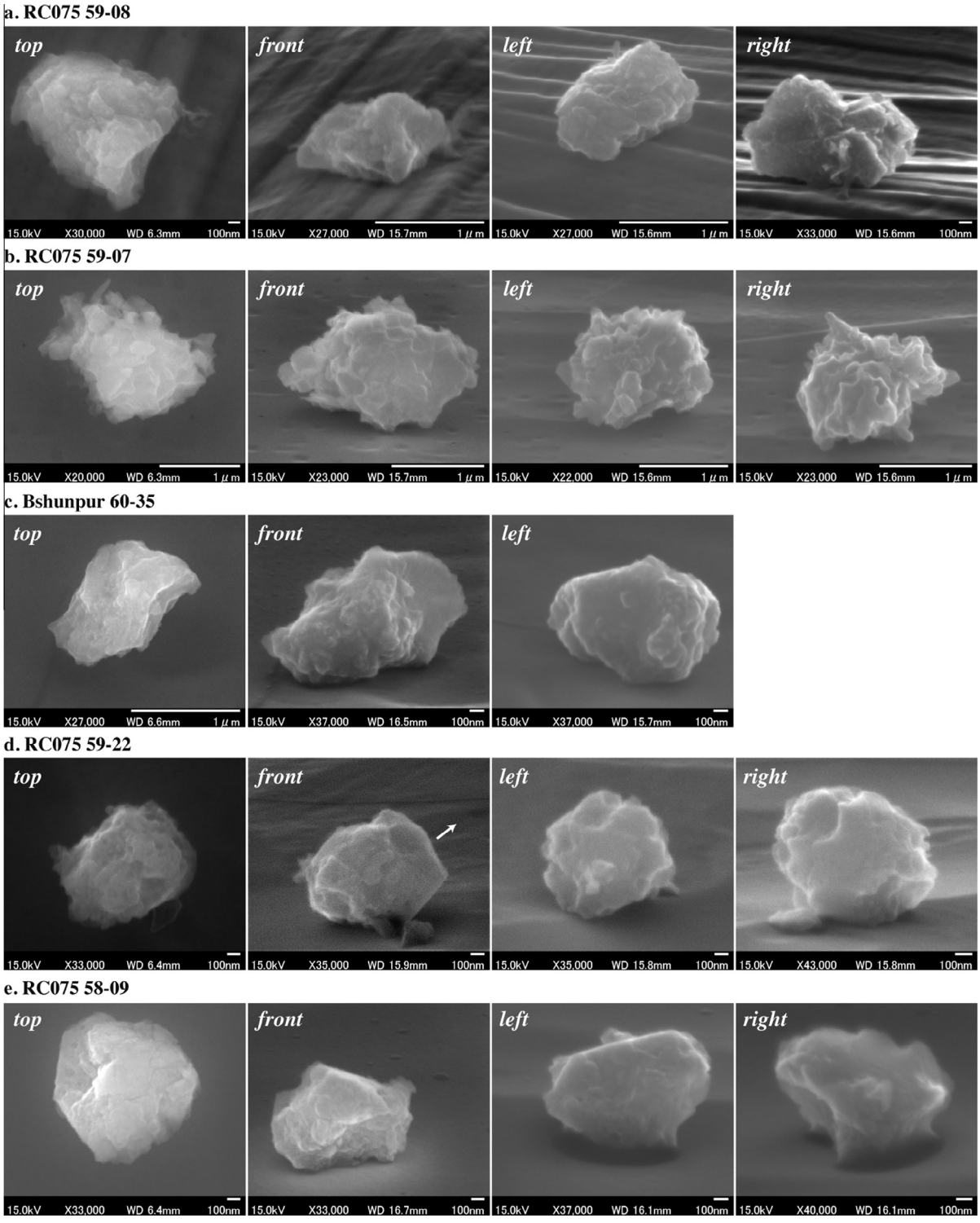

Fig. 15. Nine presolar alumina grains found from RC075 and Bishunpur. The secondary electron images of the grains were taken from four directions prior to destructive isotopic analyses by ion microprobe. (a) RC075 59-08. (b) RC075 59-07. (c) Bishunpur 60-35 (an image from the *right* direction was not taken). (d) RC075 59-22. (e) RC075 58-09. (f) Bishunpur 60-44. (g) RC075 58-49. (h) RC075 58-33. (i) RC075 59-09.

dance of presolar alumina grains is similar to that of 7% reported by Choi et al. (1998), but higher than <1% of Makide et al. (2009) and 3% of Nittler et al. (1997), in which chemical treatments of samples were basically the same as in this study. Different sampling processes and measurement techniques may have lead to the different detection probability of presolar grains. Makide et al. (2009) targeted only the large size fraction of alumina grains (1–5 μm) as

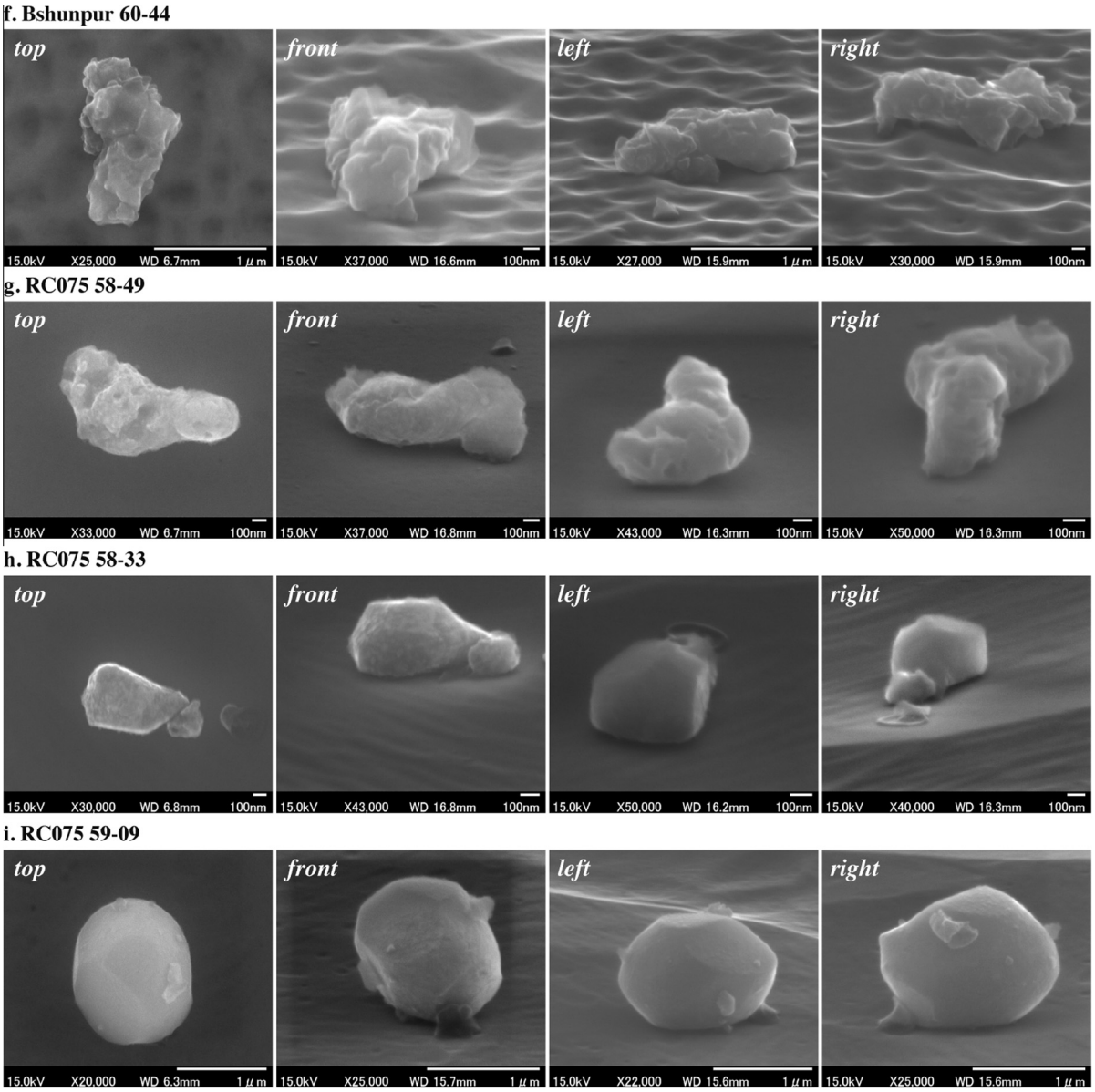

Fig 15. *(continued)*

mentioned above, and the ion mapping technique by Nittler et al. (1997) has a higher sensitivity for larger grains and grains with higher isotopic anomalies than for smaller grains with relatively less anomalous isotopic compositions, which are detectable by the methods taken in this study and in Choi et al. (1998). This could result in the relatively smaller abundances of presolar alumina grains. On the other hand, grains measured by Choi et al. (1998) and in this study could be biased towards rough-surface ones, which might result in higher proportions of presolar alumina grains.

4.2. Implications for the morphological and crystallographic characteristics of presolar and solar alumina grains

The size of presolar alumina grains found in the present and previous studies suggests that presolar alumina larger than 2 μm are scarcely present in UOCs. Absence of larger presolar alumina could be explained by growth kinetics of alumina around AGB stars and destruction efficiency of larger grains in the ISM. Expansion of high-temperature circumstellar atmospheres of AGB stars leads to the decrease of temperature and gas density. Corundum grows only while the temperature and pressure conditions of atmosphere match the supersaturation condition for corundum, and there could be a maximum grain size for circumstellar corundum. Low-velocity shockwaves by SNe effectively destroy larger grains in the ISM, because the larger grains have larger cross-sections for grain–grain collision (Jones et al., 1994, 1996). This may also set the maximum size of presolar alumina delivered to the Sun's parent materials.

Our dissolution experiments show that corundum is almost unaffected by the acid treatments of chondrites. Smooth-surface corundum grains with the solar system

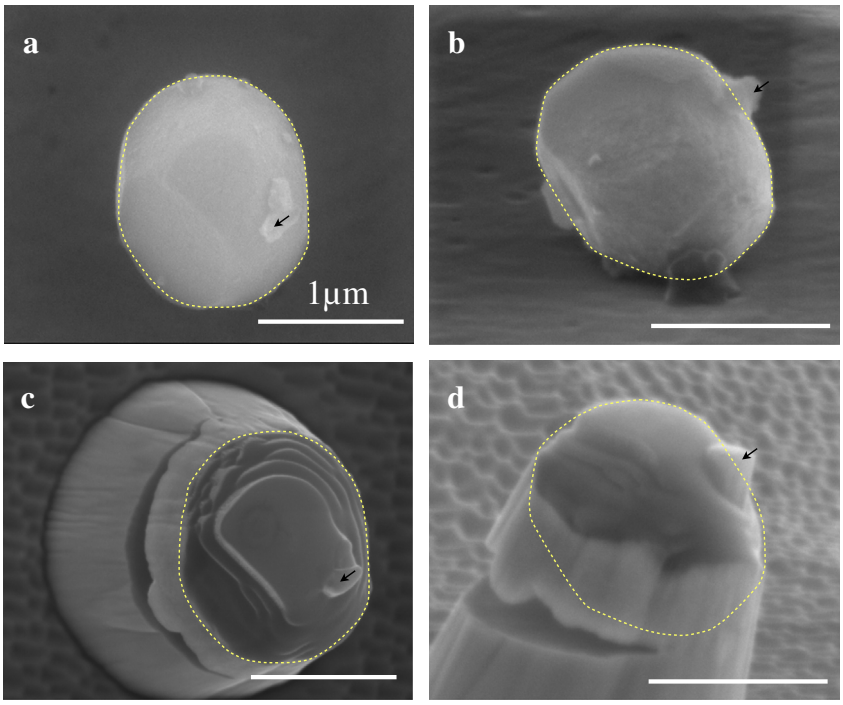

Fig. 16. Presolar alumina RC075 59-09 with sub-grains before and after the isotopic measurement. The main grain is a single crystal of α-Al_2O_3, and one of the sub-grains survived sputtering by ion microprobe is shown with an arrow. Secondary electron image of RC075 59-09 taken from the (a) *top* and (b) *front* directions before the ion microprobe analysis, and those taken from the (c) *top* and (d) *front* directions after the ion microprobe analysis. The original periphery of the main grain is shown as a dotted closed curve.

isotopic compositions (solar corundum) are likely to have not been altered since their formation in the early solar system. The rough surface structures of some solar corundum and of presolar grains may reflect the dust formation processes. However, the presence of grains having similar outer shapes but with distinct surface structures (Fig. 6) supports the idea that condensed grains originally had smooth surfaces and have been altered by irradiation with ions or low energy cosmic rays in the ISM or the protosolar disk.

Irradiation with atoms accelerated and ionized by shockwaves from SNe in the ISM has been proposed as a possible mechanism of amorphization of crystalline silicates formed around AGB stars (Jones et al., 1994, 1996; Demyk et al., 2001; Jäger et al., 2003). Circumstellar alumina grains have also been irradiated with these ions in the ISM but destruction of crystalline structure of corundum could be limited at the surface layer of grains. Irradiation experiments of corundum with Xe^+ ions showed that the critical amorphization dose of corundum is one order higher than that for forsterite (Wang et al., 1998). Transition alumina and amorphous alumina with lattice structures the same as that formed by the sol–gel method dissolve into the acid during the chemical treatments of meteorites, as shown in this study. If an acid-soluble amorphous or transition alumina layer forms around circumstellar corundum grains due to ion irradiation in the ISM, the surface altered layer would be lost during the acid treatments and rough and irregular structures could be left on the surface of corundum grains. Solar wind irradiation in the vicinity of the proto-Sun or at the surface of protosolar disk could also form similar irradiated layers surrounding solar alumina grains. The variety of surface rough structures (Figs. 5 and 6) may also be explained by the difference in degree of irradiation or irradiation condition. We should note here, however, that it is not clear how irradiation with ions destroys the crystal structure of alumina grains effectively and if the irradiated surface layer has a structure dissolvable into acids. Irradiation experiments of alumina phases have been started and preliminary results were reported by Takigawa et al. (2013).

Our dissolution experiments also indicate that transition alumina grains and amorphous alumina with the same structure as the sol–gel-formed amorphous alumina, if any, should have been completely dissolved into the acid during the acid treatments of meteorites. This is consistent with the facts that no transition alumina phases have been so far observed in chondrites and that most of alumina grains found in this study and by Stroud et al. (2004, 2007) are corundum. However, amorphous or poorly-crystalline alumina grains were found in the acid residues of UOCs in this study and by Stroud et al. (2004, 2007). This implies the presence of acid-resistant amorphous or low-crystallinity alumina, which should have different lattice structures from the sol–gel-formed amorphous alumina. A possible explanation for the acid-resistant non-corundum alumina in acid residues is that these amorphous or poorly-crystalline alumina grains include corundum-related and acid-resistant structures in a short range formed by moderate irradiation to crystalline alumina or direct condensation from a gas. Ion irradiation to corundum induces defects in its crystalline structure and destroys the crystallographic symmetry. Heavily irradiated grains or

irradiated surface layers of the grains may completely lose the original lattice structures, and may have been lost during the acid treatments. However, less irradiated grains or a deep part of irradiated grains could keep the original lattice structures in a short range and be acid-resistant. Condensation of amorphous alumina from a gas could also have different lattice structures from the sol–gel-formed amorphous alumina although lattice structures of amorphous alumina condensed under circumstellar conditions have not been well studied.

These findings also imply that undiscovered acid-soluble presolar alumina phases could be present in chondrites. Amorphous alumina produced by a sol–gel method is known to reproduce a broad peak at 11–12 μm in infrared spectra of AGB stars (e.g., Begemann et al., 1997). The presence of acid soluble alumina phases should thus be investigated in chondrites from the perspective of understanding the relationship between circumstellar dust grains and presolar grains.

5. CONCLUSIONS

Morphology and surface structures of 185 alumina grains extracted from unequilibrated ordinary chondrites (Semarkona, Bishunpur, and RC075) by chemical treatment were investigated. The ratios of the shortest to the longest dimension ranged from 0.25 to 0.75 for most grains, and neither whiskers nor extremely flat grains were present. No grains larger than 3.0 μm in size were present either. There is a variation in the shape of grains: equant, droplet-like, broken-droplet like, botryoidal, and irregular shapes. Surface structures of the grains also vary from very smooth to rough and irregular structures irrespective of grain shapes. Rough-surface grains make up about 60% of all the alumina grains, and the 10–100 nm-sized features on the rough-surface grains also vary from fluffy and edgy structures to blunt and roundish structures.

Electron-backscattered diffraction analyses of 172 grains showed that EBSD patterns of >95% of the alumina grains matched with the pattern of corundum with MAD < 1. Among 122 grains on which multiple EBSD analyses were made, identical EBSD patterns of α-Al_2O_3 were obtained from multiple locations on 75% of the grains (92 grains), showing that they are single crystals of corundum. Ten polycrystalline corundum grains were also found. There were 21 grains showing EBSD patterns with blurred or no Kikuchi bands, and they could have partially amorphous or low-crystallinity structures although the surface roughness of the grains might prevent the detection of clear EBSD patterns.

Oxygen isotopic compositions of 107 grains were measured with ion microprobe, and nine presolar grains (7 Group I and 2 Group III grains) were discovered. Seven presolar alumina grains had rough surface structures with a variety of crystallinity. Two grains were single crystals of corundum (RC075 59-22 and RC075 59-07), and one was a polycrystalline corundum grain (Bishunpur 60-44). Two grains showed EBSD patterns of corundum only from single locations and no clear EBSD patterns from other locations (RC075 58-49 and Bishunpur 60-35). Two grains (RC075 58-09 and RC075 59-08) showed only blurred EBSD patterns, where no crystalline phase was identified, and thus they were low-crystallinity or amorphous grains. Two other presolar grains (RC075 59-09 and RC075 58-33) were single crystals of corundum with smooth surfaces and were accompanied by sub-grains with fine rough structures. They could be an assemblage of solar and presolar alumina grains, and further fine-scale isotopic and structural studies are required. The fraction of rough-surface grains is higher for presolar alumina grains (at least 80%) than for solar alumina grains (~60%), which is consistent with the previous observation by Choi et al. (1998).

Dissolution experiments of synthesized transition alumina and corundum powders were made in order to evaluate the effect of chemical treatment of chondrites on the structural and crystallographic variations of extracted alumina grains. The experiments showed that corundum is almost unaffected by the acids, and that all the transition alumina phases and sol–gel-synthesized amorphous alumina easily dissolve during the acid treatments.

Morphological and crystallographic observations of presolar and solar alumina grains showed that rough-surface grains have varieties of morphology and crystallinity, suggesting that rough surfaces formed via secondary processes. Combining the results of dissolution study of alumina polymorphs, we propose that rough surface structures observed on the presolar and solar alumina grains formed by dissolution of surface layers resulting from ion irradiation in the ISM or in the protosolar disk. We also propose that acid-soluble alumina phases may be present in chondrites, but have been undiscovered due to the chemical treatments of chondrites.

The results of the present study are the first step toward understanding circumstellar dust formation and the subsequent dust evolution in the ISM and in the protosolar disk. Future statistical studies on finer-scale isotopic and structural characteristics of presolar alumina grains and experimental investigation on vapor growth of alumina and ion irradiation will help us understand the evolution history of presolar alumina grains prior to the birth of the solar system.

ACKNOWLEDGMENTS

We gratefully acknowledge Hirochika Sumino, Akihiro Kobayashi, Aya Okubo, Eric Hellebrand, Kazuhito Ozawa, and Rhonda Stroud for their help in dissolution experiments, XRD analyses, FTIR measurements, cathodo-luminescence mapping, and EBSD analyses, respectively. Careful reviews by Christine Floss and an anonymous reviewer are appreciated, which made the quality of the paper much improved. This work was supported by Grant-in-Aid for JSPS Fellows (09J02084, 12J02495) (A.T.), an Inamori Foundation research grant (S.T.), and by NASA grant NNX11AG78G (G.R.H.).

APPENDIX A. SUPPLEMENTARY DATA

Supplementary data associated with this article can be found, in the online version, at http://dx.doi.org/10.1016/j.gca.2013.09.013.

REFERENCES

Amari S., Lewis R. S. and Anders E. (1994) Interstellar grains in meteorites. I – Isolation of SiC, graphite, and diamond; size distributions of SiC and graphite. II – SiC and its noble gases. *Geochim. Cosmochim. Acta* **58**, 459–470.

Begemann B., Dorschner J., Henning Th. and Mutschke H. (1997) Aluminum oxide and the opacity of oxygen-rich circumstellar dust in the 12–17 micron range. *Astrophys. J.* **476**, 199–208.

Bernatowicz T. J., Messenger S., Pravdivtseva O., Swan P. and Walker R. M. (2003) Pristine presolar silicon carbide. *Geochim. Cosmochim. Acta* **67**, 4679–4691.

Bose M., Floss C. and Stadermann F. J. (2010) An investigation into the origin of Fe-rich presolar silicates in Acfer 094. *Astrophys. J.* **714**, 1624–1636.

Boumaza A., Favaro L., Lédion J., Sattonnay G., Brubach J. B., Berthet P., Huntz A. M., Roy P. and Tétot R. (2009) Transition alumina phases induced by heat treatment of boehmite: an X-ray diffraction and infrared spectroscopy study. *J. Solid State Chem.* **182**, 1171–1176.

Carroll-Webb S. A. and Walther J. V. (1988) A surface complex reaction model for the pH-dependence of corundum and kaolinite dissolution rates. *Geochim. Cosmochim. Acta* **52**, 2609–2623.

Choi B.-G., Huss G. R., Wasserburg G. J. and Gallino R. (1998) Presolar corundum and spinel in ordinary chondrites: origins from AGB stars and a supernova. *Science* **282**, 1284–1289.

Choi B.-G., Wasserburg G. J. and Huss G. R. (1999) Circumstellar hibonite and corundum and nucleosynthesis in asymptotic giant branch stars. *Astrophys. J. Lett.* **522**, L133–L136.

Davis A. M. and Richter F. M. (2003) Condensation and evaporation of solar system materials. In *Treatise on Geochemistry Update 1* (eds. H. D. Holland and K. K. Turekian; vol. ed. A. M. Davis). Elsevier Ltd., Oxford. pp. 1–31. Online update only.

Day M. K. B. and Hill V. J. (1953) Thermal transformations of the aluminas and their hydrates. *J. Phys. Chem.* **57**, 946–950.

Demyk L., Carrez Ph., Leroux H., Cordier P., Jones A. P., Quirico E., Raynal P. I. and d'Hendecourt L. (2001) Structural and chemical alteration of crystalline olivine under low energy He^+ irradiation. *Astron. Astrophys.* **368**, L38–L41.

Fabian D., Posch Th., Mutschke H., Kerschbaum F. and Dorschner J. (2001) Infrared optical properties of spinels: a study of the carrier of the 13, 17, and 32 μm emission features observed in ISO-SWS spectra of oxygen-rich AGB stars. *Astron. Astrophys.* **373**, 1125–1138.

Favaro L., Boumaza A., Roy P., Lédion J., Sattonnay G., Brubach J. B., Huntz A. M. and Tétot R. (2010) Experimental and ab initio infrared study of χ-, κ- and α-aluminas formed from gibbsite. *J. Solid State Chem.* **183**, 901–908.

Floss C. and Stadermann F. (2009) Auger Nanoprobe analysis of presolar ferromagnesian silicate grains from primitive CR chondrites QUE 99177 and MET 00426. *Geochim. Cosmochim. Acta* **73**, 2415–2440.

Fukuyama K., Ashida T., Okimoto K. and Ikegami H. (2009) Mechanochemical synthesis of spinel and mulite powder using transition alumina. *Res. Reports Faculty of Engineer. Kinki Univ.* **43**, 37–42.

Grossman L. (1972) Condensation in Primitive Solar Nebula. *Geochim. Cosmochim. Acta* **36**, 597–619.

Gyngard F., Zinner E., Nittler L. R., Morgand A., Stadermann F. J. and Hynes K. M. (2010) Automated NanoSIMS measurements of spinel stardust from the Murray meteorite. *Astrophys. J.* **717**, 107–120.

Hutcheon I. D., Huss G. R., Fahey A. J. and Wasserburg G. J. (1994) Extreme ^{26}Mg and ^{17}O enrichments in an Orgueil corundum: the first interstellar oxide grain. *Astrophys. J. Lett.* **425**, L97–L100.

Huss G. R. and Lewis R. S. (1995) Presolar diamond, SiC, and graphite in primitive chondrites: abundances as a function of meteorite class and petrologic type. *Geochim. Cosmochim. Acta* **59**, 115–160.

Huss G. R., Fahey A. J., Gallino R. and Wasserburg G. J. (1994) Oxygen isotopes in circumstellar Al_2O_3 grains from meteorites and stellar nucleosynthesis. *Astrophys. J. Lett.* **430**, L81–L84.

Huss G. R., Meshik A., Kehm K. and Hohenberg C. (1998) Presolar diamonds in Roosevelt county 075 and Axtell: abundances and noble-gas characteristics. *Meteorit. Planet. Sci.* **33**, A72.

Jäger C., Fabian D., Schrempel F., Dorschner J. and Wesch W. (2003) Structural processing of enstatite by ion bombardment. *Astron. Astrophys.* **401**, 57–65.

Jones A. P., Tielens A. G. G. M., Hollenbach D. J. and McKee C. F. (1994) Grain destruction in shocks in the interstellar medium. *Astrophys. J.* **433**, 797–810.

Jones A. P., Tielens A. G. G. M. and Hollenbach D. J. (1996) Grain shattering in shocks: the interstellar grain size distribution. *Astrophys. J.* **469**, 740–764.

Leitner J., Vollmer C., Hoppe P. and Zipfel J. (2012) Characterization of presolar material in the CR chondrite Northwest Africa 852. *Astrophys. J.* **745**, 38–53.

Levin I. and Brandon D. (1998) Metastable alumina polymorphs: crystal structures and transition sequences. *J. Am. Ceram. Soc.* **81**, 1995–2012.

Makide K., Nagashima K., Krot A. N. and Huss G. R. (2009) Oxygen isotopic compositions of solar corundum grains. *Astrophys. J.* **706**, 142–147.

Mendybaev R. A., Beckett J. R., Grossman L., Stolper E., Cooper R. F. and Bradley J. P. (2002) Volatilization kinetics of silicon carbide in reducing gases: an experimental study with applications to the survival of presolar grains in the solar nebula. *Geochim. Cosmochim. Acta* **66**, 661–682.

Mostefaoui S. and Hoppe P. (2004) Discovery of abundant in situ silicate and spinel grains from red giant stars in a primitive meteorite. *Astrophys. J.* **613**, L149–L152.

Nagashima K., Krot A. N. and Yurimoto H. (2004) Stardust silicates from primitive meteorites. *Nature* **428**, 921–924.

Nguyen A., Zinner E. and Lewis R. S. (2003) Identification of small presolar spinel and corundum grains by isotopic raster imaging. *Publ. Astron. Soc. Aust.* **20**, 382–388.

Nguyen A. N., Stadermann F. J., Zinner E., Stroud R. M., Alexander C. M. O'D. and Nittler L. R. (2007) Characterization of presolar silicate and oxide grains in primitive carbonaceous chondrites. *Astrophys. J.* **656**, 1223–1240.

Nittler L. R., Alexander C. M. O'D., Gao X., Walker R. M. and Zinner E. K. (1994) Interstellar oxide grains from the Tieschitz ordinary chondrite. *Nature* **370**, 443–446.

Nittler L. R., Alexander C. M. O'D., Gao X., Walker R. M. and Zinner E. (1997) Stellar sapphires: the properties and origins of presolar Al_2O_3 in meteorites. *Astrophys. J.* **483**, 475–495.

Nittler L. R., Alexander C. M. O'D., Gallino R., Hoppe P., Nguyen A. N., Stadermann F. J. and Zinner E. (2008) Aluminum-, calcium- and titanium-rich oxide stardust in ordinary chondrite meteorites. *Astrophys. J.* **682**, 1450–1478.

Onaka T., de Jong T. and Willems F. J. (1989) A study of M Mira variables based on IRAS LRS observations. I – Dust formation in the circumstellar shell. *Astron. Astrophys.* **218**, 169–179.

Ono S. and Matsuno Y. (2004) Preparation of porous alumina using CO_2 laser firing of amorphous powder synthesized by chemical solution deposition. *J. Mater. Sci.* **39**, 4367–4369.

Posch Th., Kerschbaum B. N., Mutschke H., Fabian D., Dorschner J. and Hron J. (1999) On the origin of the 13 μm feature. A study of ISO-SWS spectra of oxygen-rich AGB stars. *Astron. Astrophys.* **352**, 609–618.

Santos P. S., Santos H. S. and Toledo S. P. (2000) Standard transition aluminas. Electron Microscopy Studies. *Mater. Res.* **3**, 104–114.

Speck A. K., Barlow M. J., Sylvester R. J. and Hofmeister A. M. (2000) Dust features in the 10-μm infrared spectra of oxygen-rich evolved stars. *Astron. Astrophys. Suppl. Ser.* **146**, 437–464.

Stroud R. M., Nittler L. R. and Alexander C. M. O'D. (2004) Polymorphism in Presolar Al_2O_3 Grains from Asymptotic Giant Branch Stars. *Science* **305**, 1455–1457.

Stroud R. M., Nittler L. R., Alexander C. M. O'D. and Zinner E. (2007) Transmission electron microscopy and secondary ion mass spectrometry of an unusual Mg-rich presolar Al_2O_3 Grain. *Lunar Planet. Sci. Conf. XXXVIII*. #2203 (abstr.).

Takigawa A., Tachibana S., Nagahara H. and Ozawa K. (2012) Anisotropic evaporation and condensation of circumstellar corundum. *Lunar Planet. Sci. Conf. XXXXIII*. #1875 (abstr.).

Takigawa A. and Tachibana S. (2012) Crystallographically anisotropic shape of forsterite: new probe for evaluating dust formation history from infrared spectroscopy. *Astrophys. J.* **750**, 149–165.

Takigawa A., Matsumoto T., Miyake A., Tsuchiyama A., Nakata Y. and Yasuda K. (2013) Surface structure formation of presolar alumina (Al_2O_3): hydrogen and helium ion irradiation experiments. *Lunar Planet. Sci. Conf. XXXXIV*. #2080 (abstr.).

Wang S. X., Wang L. M., Ewing R. C. and Doremus R. H. (1998) Ion beam-induced amorphization in $MgO–Al_2O_3–SiO_2$. I. Experimental and theoretical basis. *J. Non-Cryst. Solids* **238**, 198–213.

Webster T. J., Hellenmeyer E. L. and Price R. L. (2005) Increased osteoblast functions on theta + delta nanofiber alumina. *Biomaterials* **26**, 953–960.

Wefers K. and Misra C. (1987) *Oxides and hydroxides of aluminum*. Alcoa Technical Paper No. 19, Aluminum Company of America, Pittsburgh, PA.

Zhou R.-S. and Synder R. L. (1991) Structures and transformation mechanisms of the η, γ and θ transition aluminas. *Acta Crystallogr.* **47**, 617–630.

Zinner E., Amari S., Guinness R., Nguyen A., Stadermann F. J., Walker R. M. and Lewis R. S. (2003) Presolar spinel grains from the Murray and Murchison carbonaceous chondrites. *Geochim. Cosmochim. Acta* **67**, 5083–5095.

Zinner E. (2007) Presolar grains. In *Treatise on Geochemistry Update 1* (eds. H. D. Holland and K. K. Turekian; vol. ed. A. M. Davis). Elsevier Ltd., Oxford. pp. 1–33. Online update only.

Associate editor: Anders Meibom